DRUG DELIVERY
2022, VOL. 29, NO. 1, 2644–2657
https://doi.org/10.1080/10717544.2022.2108523

Taylor & Francis
Taylor & Francis Group

RESEARCH ARTICLE

Single pot organic solvent-free thermocycling technology for siRNA-ionizable LNPs: a proof-of-concept approach for alternative to microfluidics

Anindita De and Young Tag Ko

College of Pharmacy, Gachon Institute of Pharmaceutical Science, Gachon University, Incheon, South Korea

ABSTRACT

Ionizable LNPs are the latest trend in nucleic acid delivery. Microfluidics technology has recently gained interest owing to its rapid mixing, production of nucleic acid-ionizable LNPs, and stability of nucleic acid inside the body. Industrial scale-up, nucleic acid-lipid long-term storage instability, and high production costs prompted scientists to seek alternate solutions to replace microfluidic technology. We proposed a single-pot, organic solvent-free thermocycling technology to efficiently and economically overcome most of the limitations of microfluidic technology. New thermocycling technology needs optimization of process parameters such as sonication duration, cooling–heating cycle, number of thermal cycles, and lipid:aqueous phase ratio to formulate precisely sized particles, effective nucleic acid encapsulation, and better shelf-life stability. Our research led to the formulation of siRNA-ionizable LNPs with particle sizes of 104.2 ± 34.7 nm and PDI 0.111 ± 0.109, with 83.3 ± 4.1% siRNA encapsulation. Thermocycling siRNA-ionizable LNPs had comparable morphological structures with commercialized microfluidics ionizable LNPs imaged by TEM and cryo-TEM. When compared to microfluidics ionizable LNPs, thermocycling siRNA-ionizable LNPs had a longer shelf life at 4°C. Our thermocycling technology showed an effective alternative to microfluidics technology in the production of nucleic acid–ionizable LNPs to meet global demand.

HIGHLIGHTS

- Thermocycling technology is a low-energy, low-temperature, self-assembling cooling–heating process in which lipid droplets spontaneously break apart into much smaller droplets to form siRNA-ionizable LNPs.
- The new technology is an alternative to multistep, costly, and complex microfluidics technology for the formulation and bulk up of siRNA-ionizable LNPs economically.
- Thermocycling siRNA-ionizable LNPs formulation focused on optimizing process parameters such as thermal cycle rate, number of thermal cycles, and lipid:aqueous phase ratio.
- The thermocycling technology is able to overcome the limitations of the storage stability limitations of commercialized ionizable LNPs.

ARTICLE HISTORY
Received 24 June 2022
Revised 20 July 2022
Accepted 25 July 2022

KEYWORDS
Thermocycling technology; cooling–heating cycle; siRNA; ionizable LNPs; LNPs stability

1. Introduction

Ionizable LNPs are the current trend for safely and effectively delivering nucleic acid into the body. The current example is the COVID-19 vaccines, which are massager RNA (mRNA) encapsulated in lipoplex. ONPATTRO, short interfering RNA (siRNA) loaded LNPs for polyneuropathy with familial transthyretin-mediated amyloidosis, was the stepping stone for marketed ionizable LNPs, receiving FDA clearance only in 2018. Apart from that, a vast number of clinical trials show that ionizable LNPs may be used to treat cancer, hepatitis B, influenza, zika virus, and other chronic illnesses with siRNA, mRNA, and DNA (Zhang et al., 2020; Chae et al., 2022). With the advent of genetics, these ionizable LNPs have gained a lot of attentions from the industries as a promising therapeutic tool for improving the shelf life of nucleic acid inside the body and allowing endosomal escape into targeted cells (Samaridou et al., 2020). The specific optimization of the lipid nucleic acid ratio, specific lipid aqueous phase concentration, instrument specification, ionizable lipid specification, and many other minor but critical processes parameters make these nucleic acid-ionizable LNPs a difficult and brain scratching approach for formulation scientists. Thin-film hydration, micro-emulsion, sonication, solvent injection, and other conventional methods fail to provide the requisite safety, size, shape, and bulk-up of nucleic acid–ionizable LNPs (Karnik et al., 2008; Buyens et al., 2009; Evers et al., 2018; Shepherd et al., 2021). Currently, the majority of commercialized nucleic acid–ionizable LNPs are manufactured using microfluidics technology. Microfluidics technology is a reliable and reproducible method for manufacturing nucleic acid-ionizable LNPs with exact sizes and morphologies. A laminar flow of organic solvent containing

CONTACT Young Tag Ko youngtakko@gachon.ac.kr College of Pharmacy, Gachon University, 191 Hambakmoe-ro, Yeonsu-gu, Incheon 21936, South Korea

particular lipids and an aqueous phase containing nucleic acid is forced by crossed and plunging coaxial flow and reciprocal cross mixing for the formulation of nucleic acid-ionizable LNPs. The optimization of Total Flow Rate (TFR) and Flow Rate Ratio (FRR), aqueous buffer and organic solvent ratio, rapid organic solvent removal, lipid concentration, temperature, and many other minor but critical process factors determine the exact size and morphology of microfluidics ionizable LNPs. However, because of the typical droplet production rate of 0.1–10 mL/hr, this complicated multistep process fails in bulk manufacturing and industrial scale-up to satisfy global demand (Forigua et al., 2021). The use of organic solvents in the formulation of microfluidics ionizable LNPs results in nucleic acid instability and lipid breakdown during prolonged storage (Evers et al., 2018; Roces et al., 2020). Rapid solvent removal is essential for the stability of nucleic acid, which raises manufacturing costs and increases the risk of contamination. Furthermore, the manufacturing material for the microfluidic chip, a thermoplastic with elastomer polydimethylsiloxane (PDMS), is difficult for large-scale production since PDMS absorbs nucleic acid and swells in a hydrophobic organic solvent (Tsao, 2016; Kwon et al., 2017). The application of sensitive sensors and a pump to control flow rate, mixing, and precise size makes microfluidics technology an expensive venture (Pardi et al., 2018). Furthermore, only a few others have retrofitted machinery and facilities to meet the world's need for billions of nucleic acid formulations.

Every new technology has benefits and downsides, and each new technology should be examined for its use and effect. Although microfluidic technology has a potential approach to nucleic acid delivery, it is time to develop an alternate and easy technology to solve the primary limitations of current microfluidic technology. The majority of the limitations of microfluidic technology can be overcome with single-pot, organic solvent-free thermocycling technology. A single pot technology may handle the problems of sterilization and high bulk formation without the requirement for expensive and sensitive equipment. The absence of organic solvent will overcome the limitation of long-term stability of encapsulated siRNA as well as the degradation of lipids in ionizable LNPs (Tcholakova et al., 2017). In this article, we proposed a scalable and efficient thermocycling technology based on the thermo-burst principle, in which minor temperature control is used to promote recurrent spontaneous bursting of dispersed drops into smaller droplets. It is a low-energy, low-temperature self-assemble process in which lipid droplets spontaneously break apart into much smaller droplets during thermal cycling (Tcholakova et al., 2017). Until now, the freeze–thaw cycle and phase inversion have used heat energy to encapsulate drugs and formulate vesicles by altering the thermal cycle. The biggest difference between freeze–thaw, phase inversion technology, and the newly developed thermocycling technology is the controlled and intermediate rate of the cooling–heating cycle and regulated temperature to control the morphology of droplet burst. In thermocycling technology, an optimized intermediate cooling–heating cycle only freezes the outer lipid shell but prevents the freezing of the core aqueous phase. This intermediate heating and cooling cycle creates optimized entrapped vapor pressure for the particles to burst without damaging the lipid membrane or the nucleic acid. Whereas in freeze-drying and phase inversion methods, particles break due to the crystallization stress during the freeze–thaw cycle, which damages the lipid membrane and encapsulated therapeutics, making it unsuitable for nucleic acid delivery (Abdelwahed et al., 2006; Trenkenschuh & Friess, 2021). The thermocycling technology creates a flexible intermediate elasto-plastic phase of isotropic liquid which generates a high vapor zone within the particles for thermos-bursting (Cholakova et al., 2020). Partial mobility of molecules assembled in the rotator phase during thermal cycling, allowing for molecular exchange and dynamic equilibrium with neighboring liquid lipid molecules, resulting in nano-size ionizable LNPs (Valkova et al., 2017). The thermocycling technology for the formulation of siRNA-ionizable LNPs is depicted schematically in Figure 1 and is one of the first-time approaches for the formulation of ionizable LNPs without any organic solvent.

As a proof of concept, we demonstrated that the research process was rather universal, scalable, and cost-effective. For this study, we used a gold standard ionizable-helper lipid–cholesterol-PEG-lipid combination that was used for ONPATTRO (Microfluidic technology-based LNPs). We use universal scrambled siRNA (AccuTarget™) for process parameter optimization because the project focused on the optimization of a novel technology. We took a number of process permanents and optimized them one by one to formulate siRNA-ionizable LNPs with a similar size, shape, encapsulation, and release profile as the FDA-approved marketed ONPATTRO ionizable LNPs. These systems, on the other hand, serve as a new type of versatile toolbox for investigating minimal-in-composition systems in order to reduce the healthcare cost burden in developing and undeveloped countries.

2. Materials

2.1. Lipids phase

Ionizable lipid: D-LinMC3-DMA procured from Medchem Express, **Helper lipid**: 18:0 PC (DSPC) (1,2-distearoyl-sn-glycero-3-phosphocholine), **Stabilizer lipid:** Cholesterol and **PEG-Lipid:** DMG-PEG 2000 (1,2-dimyristoyl-rac-glycero-3-m ethoxypolyethylene glycol-2000) were purchased from Avanti Polar Lipids, Inc. The lipid mixture melting temperature ranges from 30 to 65 °C and freezing at 12–8 °C in the mixed state. All studied lipids are approved by FDA, USA, and used as received.

2.2. Aqueous phase

Universal scrambled siRNA (AccuTarget™) procured from Bioneer (Daejeon, South Korea) (pH 4.5, 20 mM citrate buffer). All aqueous solutions were prepared with deionized water. All materials were used without further purification and modification.

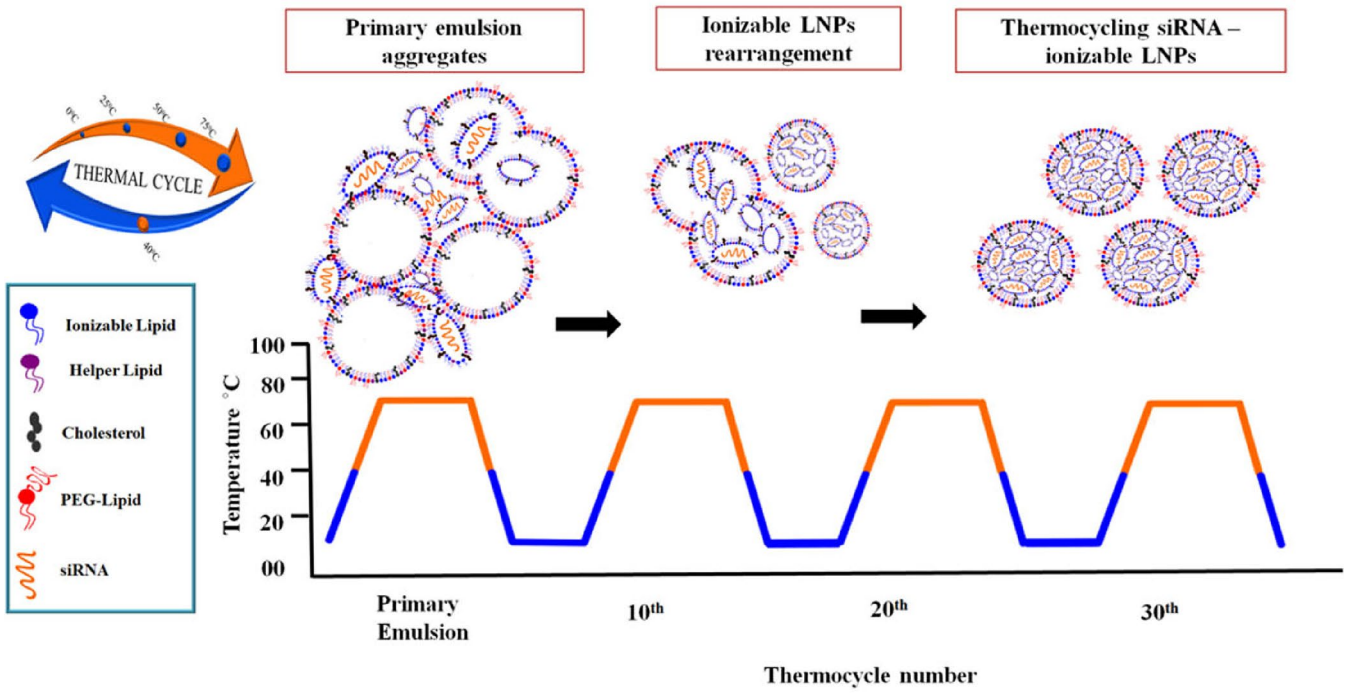

Figure 1. Schematic representation of formulation of thermocycling siRNA–ionizable LNPs by simple change in cooling–heating cycle.

3. Formulation and optimization of thermocycling siRNA-ionizable LNPs

3.1. Primary emulsion formation

A coarse oil-in-water emulsion was formed in a single vial by simply mixing and stirring at 1200 rpm at 70 °C for 24 hrs (Golmohammadzadeh et al., 2012). The lipid phase contained D-LinMC3-DMA, DSPC, Cholesterol, and PEG-DSPE(2000) in a molar ratio of 50:10:38.5:1.5, which was similar to the FDA approved ONPATTRO LNPs. 8.8 µg of scramble siRNA (AccuTarget™) was dissolved in 200 µL of 20 mM citrate buffer pH 4.5 to form the aqueous phase. The N/P ratio of the lipids and siRNA was 6. Throughout the mixing, the temperature was kept 5 °C above the bulk melting point of the lipid mixture. Finally, the mixture was frozen at 5 °C to solidify the lipid shell but not the core aqueous phase (Denkov et al., 2015; Tcholakova et al., 2017; Valkova et al., 2017). Particle size (PS) of the primary emulsion was determined using dynamic light scattering (DLS) (Photal, Osaka, Japan). Bath sonication was used to achieve initial PS reduction and homogeneity.

3.2. Optimization of bath sonication time

The bath sonication time was optimized for 3, 6, and 9 minutes (mins) to investigate the sonication effect on primary emulsion PS reduction (Cun et al., 2010; Kundu et al., 2012). We also consider siRNA stability during the emulsification and sonication processes. The ultrasonic bath (Branson® ultrasonic cleaner, 2510, Branson Ultrasonic Corp., CT, USA, 1.91 L) does not allow for amplitude adjustment and was used at the manufacturer's power level. The bath sonication specifications chosen for this study were 20 kHz ultrasound frequency, angular frequency of 125,600 rad/s, the input power of 32 W, the density of liquid of 998 kg/m^3, and sound velocity of liquid maintained at 1500 m/s (Cun et al., 2010). Only the time parameter was adjusted to investigate the influence of bath sonication on size reduction and uniformity. The PS and polydispersity index (PDI) of the formulation were evaluated in the presence or absence of bath sonication (Mean SD, $n = 3$).

We used a thermos Fisher mini ampere PCR machine with a customized thermocycling design to critically optimize each process parameter to obtain the final optimized formula for thermocycling siRNA-ionizable LNPs with precise size, high loading, and long-term storage stability. The following was the thermocycling procedure:

1. The cooling procedure began at a temperature at least 5°C higher than lipid mixer bulk melting temperature. The solution cooled at optimized rate. The process temperature reduced until the dispersed lipid droplets shells were completely frozen.
2. The melting of the drops were done at an optimized rate. The temperature of the system was increased until it reached the specific heat, which caused all of the dispersed lipids to become liquid. Optimized heating and cooling cycle was repeated until the desired PS was achieved and the high concentration siRNA entrapped inside the ionizable LNPs.
3. The impact of thermal stress, thermal compatibility, and the number of thermal cycles were carefully optimized for specific sized, high-entrapped, and stable ionizable LNPs.

3.3. Optimization of cooling–heating rate for thermocycling technology

Heating and cooling rates were optimized for thermocycling siRNA-ionizable LNPs. The lipid mixture had a melting point of 65 °C and a freezing point of 8 °C. A rapid cooling and rapid heating (5 °C ↔70 °C), (No intermediate point between the rapid heating and cooling was used), slow cooling (cooling rate 5 °C/mins) rapid heating (heating rate 70 °C/mins), and intermediate cooling–heating were used to evaluate PS reduction and PDI of ionizable LNPs. The intermediate heating and cooling temperatures were chosen based on droplet shape transformation into solid frozen particles without lipid member deformation and PS (Denkov et al., 2015; Tcholakova et al., 2017; Valkova et al., 2017).

3.4. Optimization of thermocycle number for thermocycling technology

The number of thermocycle was another important parameter to optimize for successful size reduction, siRNA entrapment, and siRNA stability inside the ionizable LNPs during the thermocycling technology. We investigated the effects of 10, 20, 30, and 40 thermocycle on the size, shape, and entrapment of siRNA and compared them to ONPATTRO LNPs data.

3.5. Optimization of lipid–aqueous phase ratio of thermocycling technology

The lipid:aqueous phase ratio played a structural and stabilizing role in the formation and encapsulation of siRNA during the continuous thermocycling process. The effect of the phase ratio on PS, PDI, morphology, and stability of thermocycling siRNA-ionizable LNPs was investigated using 1:10, 1:20, 1:30, 1:40, and 1:50 lipid:aqueous phase ratios.

3.6. Evaluation of size, potential and morphology of thermocycling siRNA-ionizable LNPs

PS and PDI were measured using DLS technology. To get the best scattering intensity, thermocycling siRNA-ionizable LNPs were diluted with water. For data point analysis, the hydrodynamic diameter, PDI, and zeta potential were measured at 25 °C at a 90° angle in ELS-Z (Photal, Osaka, Japan) with a viscosity of 0.898 cP and a refractive index of 1.332. The device was calibrated regularly with a latex suspension (262 nm, 112 nm; Photal, Otsuka electronics, Osaka, Japan).

Transmission Electron Microscopy (TEM) and cryogenic TEM (cryo-TEM) images of thermocycling siRNA-ionizable LNPs were used to examine the morphology. A TEM and cryo-TEM sample was made using a thin aqueous layer supported by a holey carbon grid. TEM and Cryo-TEM data were collected using a 200 kV Tecnai F20 (FEI, Netherlands) temperature of around −170 °C. All images were captured with an FEI Eagle 4 K CCD camera mounted on the bottom. All samples were photographed at magnifications of 14.5 K and 25 K (scale bar 50 nm and 20 nm), with a notional under-focus of 1–2 µm.

3.7. Evaluation of siRNA encapsulation in thermocycling ionizable LNPs

The gel electrophoresis assay was used to study encapsulation efficiency and stability of siRNA inside thermocycling ionizable LNPs. Naked siRNA was used as a control. Thermocycling siRNA-ionizable LNPs with an equivalent weight of 0.44 µg in 9 µL mixed with 1 µL (10×) loading dye (GenDEPOT pink safe) utilized as the sample. The standard and prepared samples were run through 1% w/v agarose gel and Tris-borate (1XTBE) buffer at 50 V for 10 mins at 25 °C. The electrophoretic mobility of GenDEPOT pink safe dyed was examined using an ultraviolet (UV) illuminator (GelDoc, Bio-Rad, USA). Triton X100 (0.2%) was used to lyse the ionizable LNPs. The mobility and stability of siRNA encapsulated inside the thermocycling ionizable LNPs were compared using gel electrophoresis data.

The Quant-iTTM PicoGreen® reagent (Invitrogen) (Cui, 2015; Cui et al., 2022; Ryu et al., 2022) was used to quantify siRNA inside thermocycling ionizable LNPs. Standard curve of siRNA (1 ng/mL–1 µg/mL) at pH 7.4 was constructed. 50 µL of thermocycling siRNA-ionizable LNPs (theoretical value 44 µg/1 mL) and 50 µL of PicoGreen reagent was mixed to a 96-well plate. A multi-plate reader (BioTek Synergy H1 Multimode Reader) was used to quantify fluorescence intensity at 485 nm excitation and 525 nm emission wavelengths. The siRNA entrapment efficiency was calculated using the formula:

$$\%\ \text{Entrapment efficiency} = \frac{\text{Total amount of siRNA} - \text{unencapsulated siRNA}}{\text{Total amount siRNA}} \times 100$$

3.8. Evaluation of siRNA release from thermocycling ionizable LNPs

The release of siRNA from thermocycling ionizable LNPs at 37 ± 2 °C in PBS pH 7.4 and pH 5.5 was evaluated using a dialysis tube (MWCO 25 kDa, Gene Bio- Application LTD, Israel). The pH of 7.4 mimics the normal body or cytoplasmic condition, whereas the pH of 5.5 mimics the endosomal pH, to understand the fate of thermocycling siRNA-ionizable LNPs. 50 µL of formulation was placed in the dialysis tube and immersed in 3 mL of PBS solution under 100 rpm. The sample collected periodically until the siRNA was completely released. siRNA release was quantified by the fluorescence intensity of Quant-iTTM PicoGreen® reagent (Invitrogen) at each time interval. The stability of siRNA during the release study was confirmed by agarose gel electrophoresis.

3.9. Evaluation of serum stability of thermocycling siRNA-ionizable LNPs

The serum nucleases degrade siRNA, making it highly unstable (Bakhtiar et al., 2022). The stability of siRNA was tested in 10% (v/v) fetal bovine serum (FBS) and compared to naked siRNA and serum-free conditions. Naked siRNA (0.44 µg) and thermocycling siRNA-ionizable LNPs 10 µL

(equivalent to 0.44 µg siRNA) incubated with an equal volume of DMEM (Dulbecco's Modified Eagle Medium) comprised of 10% (v/v) FBS at 37 ± 0.5 °C and gently vortexed. At defined time intervals, i.e. 0, 0.5 1, 2, 4, and 6 hrs, samples were taken and stored at −80 °C. When the last aliquot collected at 6 hrs, gel electrophoresis was performed to confirm the siRNA stability.

3.10. Evaluation of storage stability of thermocycling siRNA-ionizable LNPs

One of the most serious concerns with current nucleic acid-ionizable LNPs is their short storage period and stability during long-term storage (Jones et al., 2007; Suzuki et al., 2015; Ball et al., 2017; Moderna, 2020; Zhao et al., 2020). Use of the organic solvent is one of the causes of the ultra-low storage temperature of the commercialized ionizable LNPs (Ball et al., 2017; Zhao et al., 2020). Trace amount of organic solvent (2–5%) present inside the ionizable LNPs causes lipid and nucleic acid degradation during prolonged storage. The absence of any kind of organic solvent in thermocycling technology may improve the stability and shelf life of thermocycling siRNA-ionizable LNPs. Thermocycling siRNA-ionizable LNPs were stored at 25 °C (room temperature), 4 °C (refrigerator), or −21 °C (freezer) temperatures for 3 months. The formulations were brought to room temperature for measurements at predetermined intervals, and the bulk solutions were then returned to their original temperatures for storage. During 90 days, the thermocycling siRNA-ionizable LNPs were measured for size and PDI.

4. Results and discussion

4.1. Optimization of bath sonication time for primary emulsion

Sonication energy disperses primary emulsion PS and breaks up agglomerates. The encapsulating siRNA can also be destroyed by prolonged sonication(Kumar et al., 2018). The purpose of sonication was to form a monodispersed primary emulsion. PS and PDI changes were evaluated to understand the impact of sonication (Mean SD, $n = 3$). The integrity of the siRNA during the sonication period was observed by gel electrophoresis.

As expected, increasing the sonication time effectively breaks down the lipid aggregates and reduces PS (Table 1). After 6 mins of sonication, the average cluster size reduced from 2167.6 ± 510.2 nm (for 0 min i.e. without sonication) to 472.5 ± 169.6 nm. Further sonication for 9 mins lowered the PS to 441.7 ± 82.6 nm, but gel electrophoresis showed damage to entrapped siRNA. Sonication for more than 9 mins had no appreciable effect on PS reduction but entirely damaged the encapsulated siRNA (Figure 2). Sonication was only employed to emulsify lipids in the aqueous phase. Sonication was an intermediary phase that did not result in the final product. With the onset of sonication, the average cluster size decreased quite fast, and the homogeneity of the PDI was also observed. Finally, a sonication time of 6 mins was chosen to develop a monodispersed primary emulsion as it effectively reduced the PS without damaging the siRNA.

4.2. Optimization of cooling–heating rate of thermocycling technology

The rate of the heating and cooling cycle was one of the most important requirements in thermocycling technology. The rate of heating and cooling had a direct effect on the lipid shell solidification and rearrangement during the thermocycling process without freezing the internal fluid core. The rate of the thermal cycle determined the PS, shape, and long-term stability of the formulation.

The rapid cooling–heating (5 °C ↔70 °C) (Figure 3A) causes the particles to crack and reformed but the reduction of the PS was not much. The rapid cooling and heating behaved like a freeze–thaw cycle. The frozen particles crack during the freezing phase due to the expansion of the solidified aqueous phase, which increases the PS during the thaw cycle. The hydrophobic core fuses during the rapid cooling process to form an aggregate-like structure, which reduces structure lamillarity and induces size expansion (Sriwongsitanont & Ueno, 2010). Owing to rapid temperature fluctuations (5 °C ↔70 °C), hydrated lipids heads turned dehydrated and aggregated. The aqueous phase does not have enough time to penetrate within the lipid aggregation to break it apart during rapid (5 °C ↔70 °C) thermal cycle, resulting in larger PS. A rapid cooling–heating (5 °C ↔70 °C) process proved unsatisfactory for size reduction in thermocycling technology.

The size decrease was very much negligible for the slow cooling (5 °C/min) and rapid heating (70 °C/min) cycles (Figure 3B). Long contact between the aqueous phase and the lipid phase, during the slow cooling process, results in large lipid crystal domain formation. However, because the rapid heating could not generate enough vapor pressure to break the stable crystal domain, the reduction of the PS was negligible. Slow cooling (5 °C/min) and rapid heating (70 °C/min) were inefficient for thermocycling siRNA-ionizable LNPs formulation, as illustrated in Figure 3(B).

A range of heating (50 °C/mins, 40 °C/mins, 30 °C/mins) and cooling (15 °C/mins, 25 °C/mins, and 35 °C/mins) temperatures were investigated for the selection of intermediate heating and cooling conditions for thermocycling technology. When the cooling rate varies between 15 °C/mins, 25 °C/mins, and 35 °C/mins (heating kept constant at 70 °C/min), the drop freezing into solid particles occured at a different rate. The slow cooling led to freezing at a very late stage and had the high lipid water interaction to form stable

Table 1. Effect of sonication time on particle size of siRNA-ionizable LNPs.

Sonication time	0 min	3 min	6 min	9 min	12 min
PS (nm)	2167.6 ± 510.2	1132.7 ± 323.8	472.5 ± 169.6	441.7 ± 82.6	438.9 ± 61.5
PDI	0.811 ± 0.213	0.611 ± 0.219	0.114 ± 0.202	0.119 ± 0.105	0.189 ± 0.0264

spherical-shaped droplets. But a very slow cooling rate like 15 °C/mins (Figure 4A,B) produced a very stable large size of the lipid crystal domain, which was difficult enough to break apart uniformly. During the heating cycle, the bursting of the droplets was not uniform and big and large droplets evolved that affected the thermos-bursting during the heating cycle. At a higher cooling rate (35 °C/min), the big drops tended to freeze into spherical solid particles without shape transformations, while the smaller drops readily evolved in shape, leading to high PSdistribution. But when we checked the intermediate heating rate of 25 °C/mins, we observed the PS freezing uniformity and the PS distribution intensity was better than the 15 °C/mins and 35 °C/mins. The stable elasto-plastic phase of lipids within the intermediate cooling rate creates flexible lipid curvature to form the homo-dispersed PS after the thermocycling. So we can conclude that an intermediate 25 °C/min was able to produce sufficient time and contact period to form a uniformly frozen droplet size for the heat cycle (Denkov et al., 2015; Tcholakova et al., 2017).

The heat cycle depends on the cooling cycle. When an intermediate cooling rate (25 °C/mins) and high heating (50 °C/mins) (Figure 4C,D) were used the PS bursting rate was too poor. The reason may be the less heating cycle contact time to break apart the large crystal domain of the frozen particles. The decrease in the heat cycle (30 °C/mins) effectively reduces the PS, but the generation of the big and small PS alters the PS distribution and homogeneity. The reason was non-uniform generation of the vapor pressure within the lipid crystal domain and the generation of more vapor pressure within the particles for the thermos-burst non-uniformly (Denkov et al., 2015; Tcholakova et al., 2017; Valkova et al., 2017; Cholakova et al., 2020). The intermediate heating cycle (40 °C/mins) with the intermediate cooling cycle (25 °C/mins) was found to be appropriate for the droplet breakdown and uniform size distribution.

When intermediate rapid cooling (40 °C/mins) was followed by intermediate slow heating (25 °C/mins), effective particle disintegration was observed. The intermediate rapid cooling ensures the formation of the smaller lipid crystalline domain in the frozen lipid shell. Slow solidification and rearrangement of the lipid shell without freezing the core aqueous phase was a crucial and critical optimization procedure. The aqueous phase effectively penetrated the lipid particles by intermediate and slow heating, resulting in optimal vapor pressure for efficient PS reduction by thermos-burst without compromising the stability of the encapsulated siRNA (Tcholakova et al., 2017; Valkova et al., 2017; Sato, 2018; Cholakova et al., 2020). For the next experiment parameters, the intermediate heating and cooling strategy (Figure 3C) was adopted as it was shown to be the most successful for the formation and stabilization of thermocycling siRNA-ionizable LNPs.

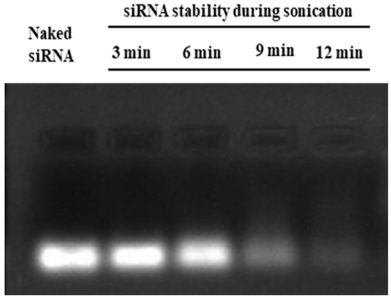

Figure 2. Stability of thermocycling siRNA-ionizable LNPs: Encapsulated siRNA was found stable till 6 mins of sonication but with increase time of sonication siRNA found unstable. Lane 1- Naked siRNA, Lanes 2–5 Triton X100 lysate thermocycling siRNA–ionizable LNPs.

4.3. Optimization of thermocycle number for thermocycling technology

The number of thermocycles is another important process parameter in thermocycling technology. The number of thermocycles affects the stability of both siRNA and lipids. Thermocycling siRNA-ionizable LNPs PS and shape were optimized by utilizing a series of thermal cycles. Thermocycling technology was developed with primary (0^{th}), 10^{th}, 20^{th}, 30^{th}, and 40^{th} cycle numbers, and the size of thermocycling siRNA-ionizable LNPs was compared to the volume intensity and number distribution (Figure 5A,B). The study discovered that after the 10^{th} cycle, thermocycling siRNA-ionizable LNPs with a volume-average diameter (d_V) ≈ 255.9 ± 65.2 nm and number-average diameter (d_N) ≈ 249.7 ± 35.7 nm showed a significant drop in PS compare to the primary PS (d_V)

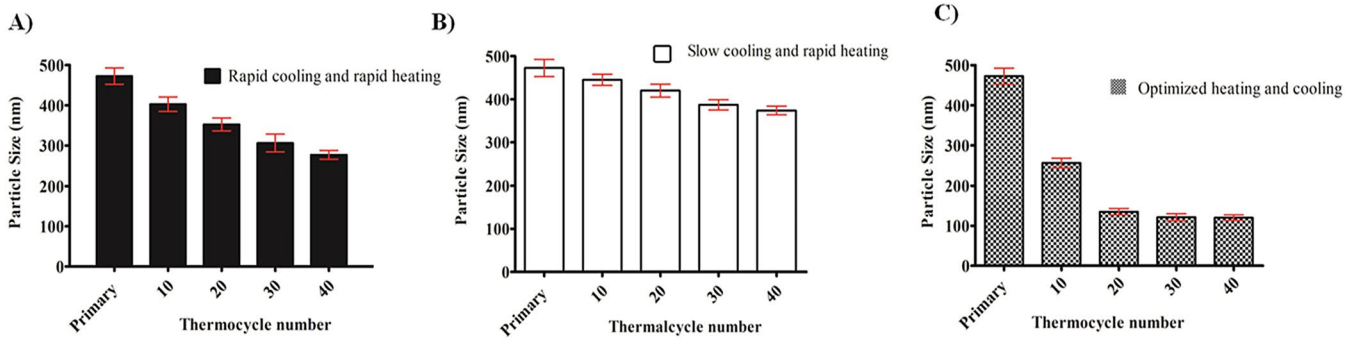

Figure 3. Optimization of thermocycle temperature: Different thermocycling conditions have a strong impact on PS. (A) Rapid cooling and rapid heating cycle able to reduce the PS but not effective enough to reduce the PS <200 nm. (B) The slow cooling and rapid heating not at all effective for the size reduction of ionizable LNPs as the heat was not sufficient enough to break the stable crystal domain. (C) Intermediate optimized rapid cooling and slow heating effectively reduce the PS in the range of 134.9 ± 11.7 nm by the optimized heating and the cooling rate ($n = 4$, Mean ± SEM).

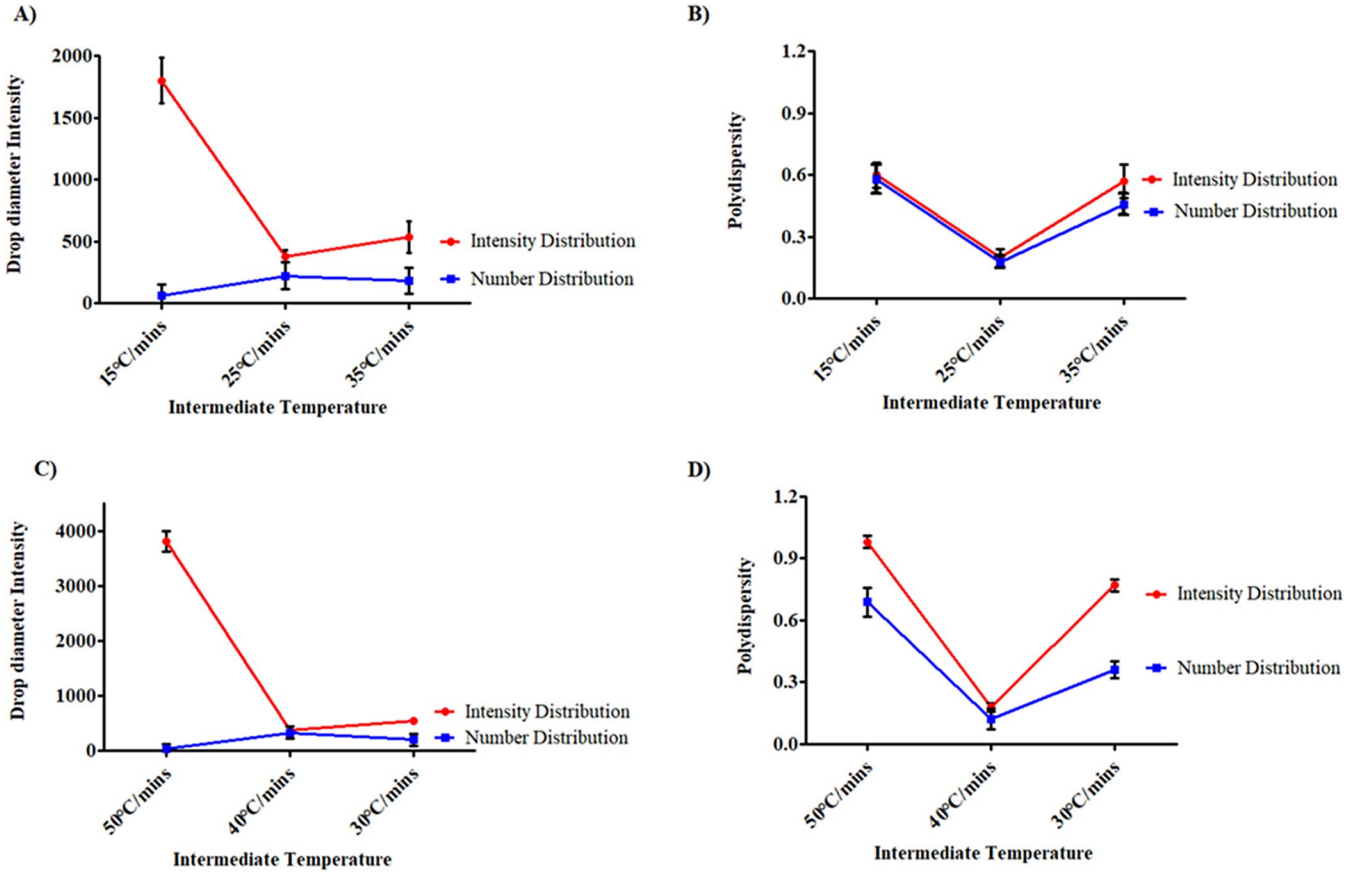

Figure 4. Selection of intermediate cooling–heating cycle. (A) At a slow cooling rate15 °C/mins the particle size intensity distribution is very high and low number distribution indicate the formation of large particle size which significantly reduce at cooling rate 25 °C/mins. (B) The PDI data correlated with the size distribution data, at slow cooling rate high PDI indicate the formation of big and small particles with non-uniform distribution. (C) At a high heating rate also the large particle size droplet intensity which reduce with slow heating rate. (D) the PDI was found uniform with optimized heating rate of 40 °C/mins. ($n = 4$, Mean ± SEM).

472.5 ± 169.6 nm and (d_N) 468.8 ± 125.3 nm. After the 20th thermocycle, d_V decreased to ≈134.9 ± 11.7 nm and d_N to ≈ 131.6 ± 23.4 nm. The detected decrease sizes were d_V ≈ 131.5 ± 5.6 and d_N ≈ 130.6 ± 43.9 nm after the 30th thermocycle, and d_V ≈ 138.2 ± 69.4 nm and d_N ≈ 137.2 ± 89.7 nm after the 40th thermocycle, which did not change significantly from the 20th cycle.

The dramatic reduction in PS was connected with the optimized contact duration between the aqueous phase and the lipid phase, which substantially reduced the PS from the primary to the 10th cycle (Tcholakova et al., 2017; Valkova et al., 2017; Cholakova et al., 2020). We also investigated the thermal cycle with the 1st, 3rd, and 5th cycles but observed that they were ineffective in lowering PS (data not shown). We concluded from the experiment that a minimum of 10 thermocycles were necessary for successful PS reduction. The effective 10th cycle was able to provide appropriate heating and cooling conditions for optimal aqueous phase penetration into the lipid crystal domain, as well as adequate vapor pressure generation for the thermos-burst and droplet breakdown. Figure 5(A,B) corresponds with the data, demonstrating that as the thermal cycle number increases, so does the number distribution, indicating a drop in PS and a decrease in the intensity distribution associated with particle aggregation rates. An intermediate thermal cycle of the 12th, 15th, and 17th thermal cycles were tried in between the 10th and 20th cycles for a more specific understanding of the thermos-bursting concept. The 12th (d_V ≈247.3 ± 8.7 nm and d_N to ≈ 243.4 ± 33.4 nm) and the 15th cycle (d_V ≈226.1 ± 15.8 nm and d_N to ≈ 221.4 ± 16.2 nm) did not show any significant changes but a rapid decreased in PS was observed in 17th cycle (d_V ≈158.5 ± 17.9 nm and d_N to ≈ 155.3 ± 17.2 nm). Prolongation of the contact time enhances the thermos-bursting of the lipid droplets and can reduce the PS. However, there was little evidence of a reduction in PS beyond the 20th cycle. The exact reason for this is still unclear. The aqueous phase concentration impact on the PS reduction might be a possible explanation. The dramatic fall in the PDI in the 10th and 20th cycles suggests that the particles become more monodispersed as the thermocycle number increases, while a rise in the PDI in the 30th and 40th (Figure 5B) cycles may indicate the formation of aggregates owing to lipid lamillarity loss. As a result, the 20th cycle was optimized for the formation and size reduction of thermocycling siRNA-ionizable LNPs.

We used TEM pictures of the primary, 10th, 20th, and 30th cycles (We skipped the 40th cycle since the 30th thermal cycle alters the morphology of the siRNA-ionizable LNPs) to verify our theory that the number distribution increases but the intensity distribution decreases as the number of

thermocycles increases. Figure 5(C) shows illustrative TEM images of alterations in the PS number distribution that support the DLS results. The TEM results also demonstrated that a simple thermocycle technology is efficient enough for PS reduction and may be a potential alternative to microfluidics technology.

Thermocycle refers to the minute changes in cooling–heating that cause the lipid layer to deform and regenerate with each cycle. Changes in morphology of the thermocycling siRNA-ionizable LNPs were very much observed with the changes of each thermocycle (Figure 6). A noticeable alteration in the shape of the lipid droplets was observed in the 30th cycle. Prolonged thermal cycle exposure may alter the lipid layer of the lipid crystallization domain. A change in hydration as a result of long-term exposure to high temperatures might be the cause of the changes. When the number of heat cycle exposures was low (10th and 20th), the head-group of lipids was well hydrated, but as the cycle number increased (30th and 40th), it became more dehydrated, causing the lipid structure to deform (Vandamme & Anton, 2010; Chuesiang et al., 2018). The TEM image also supports

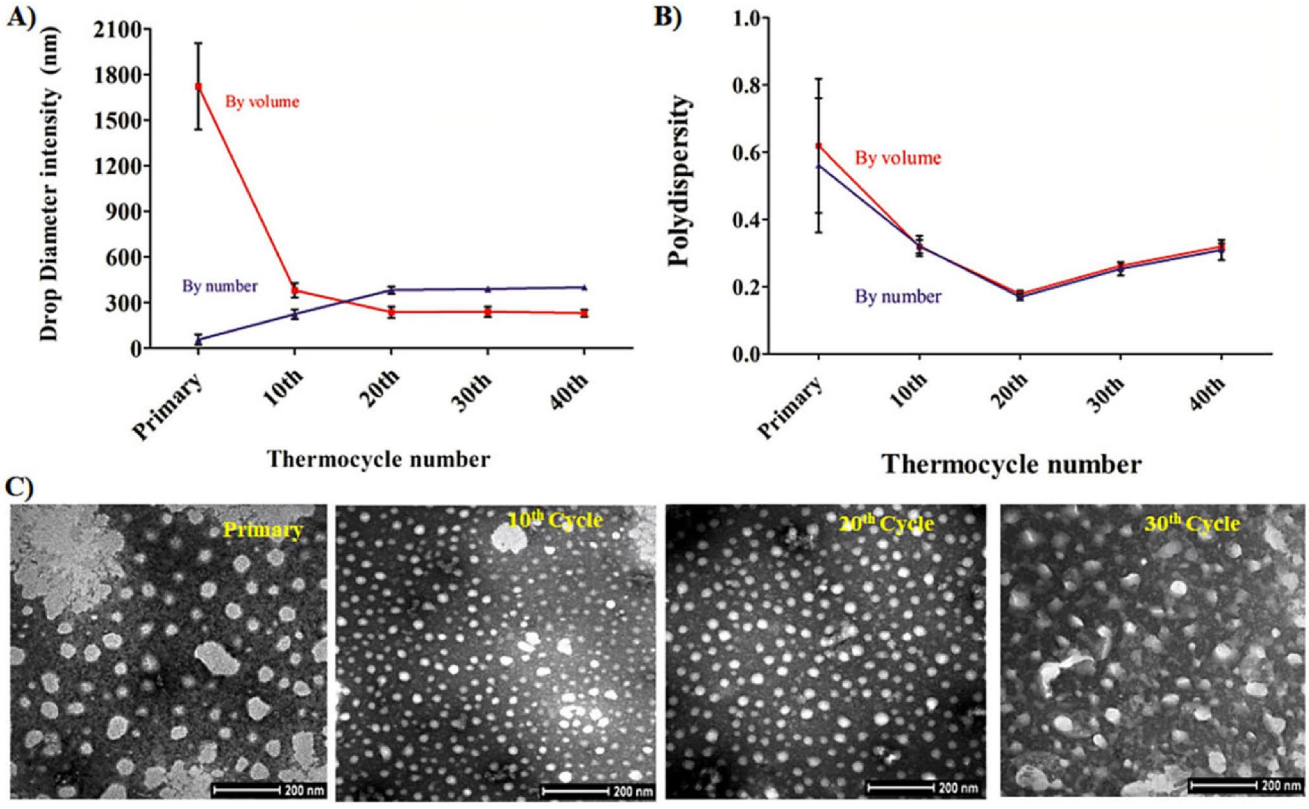

Figure 5. Optimization of the number of thermocycle: The number of the thermocycle had a critical effect on the PS reduction. The study was performed with initial drop diameters of 472.5 ± 169.6 nm. (A) the increase in the number intensity and the reduction of the distribution intensity clearly showing that the number of the thermal cycle able to reduce the PS of ionizable LNPs by simple thermoburst. (B) The siRNA ionizable LNPs polydispersity showing the change during the increase in the thermal cycle support the concept of mono-dispersity with increasing the cycle number. ($n = 4$, Mean ± SEM). (C) TEM images of the siRNA loaded ionizable LNPs in different thermocycle (scale bar: 200 nm). The primary emulsion aggregates size reduces with increase number of thermal cycle correlated with the DLS data. (DLS provide the hydrodynamic size (Nps size + liquid layer) TEM gives the dry particle size).

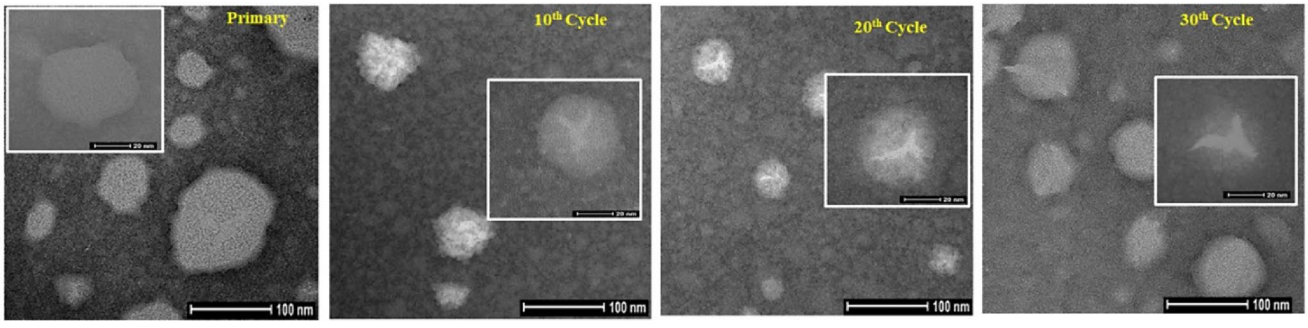

Figure 6. Morphological changes during thermocycle: Prolonged exposure in thermocycle disturbed the outer layer of the ionizable LNPs and causes to loose of the specific shape of the lipid layer (scale bar = 100 nm) and insert TEM image of indicate deforms outer membrane of the thermocycling siRNA-ionizable LNPs (scale bar= 20 nm).

the 20th cycle as the optimum thermocycle number for future work.

4.4. Optimization of lipid–aqueous phase ratio for thermocycling technology

While optimizing the thermocycling technology parameters, we observed that the lipid hydration state, internal core size, and lipid:aqueous phase ratio all played important roles in the optimal size, shape, and stability of the thermocycling siRNA-ionizable LNPs (Table 2). The formation of vapor pressure for thermos-burst depends on the internal aqueous phase concentration during thermocycling. We altered the lipid aqueous phase ratio while keeping the other optimized parameters constant, to simulate the effect of changing the aqueous phase ratio during thermocycling. A volume ratio of 1:10 produced the largest PS and PDI, 147.7 ± 104.6 nm and 0.492 ± 0.216 respectively. The volume ratios of 1:20 and 1:30 produced very similar PS of 109.5 ± 84.9 nm and 104.2 ± 34.7 nm with PDI of 0.215 ± 0.358 and 0.111 ± 0.019, respectively. The PS values of 114.7 ± 14.2 nm and 134.9 ± 100.6 nm and 0.181 ± 0.104 and 0.178 ± 0.283 PDI changed radically when the aqueous phase ratio increased to 1:40 and 1:50.

The concentration of lipids and PEG-lipids, as well as the produced vapor pressure inside the frozen lipid shell, were affected by the volume of the aqueous phase. The PS increased as the aqueous phase of the thermocycling siRNA-ionizable LNPs formulation changed. Initially, the disintegration of frozen lipid particles into numerous little lipid particles depended on the original drop size of the primary emulsion. But with increasing temperature, the process becomes more intense and crests greater internal pressure to burst into nano-sized lipid droplets. The head-group of lipids was highly hydrated at relatively low temperatures or fewer thermal cycles but became gradually dehydrated with increased heat exposure and evaporation of the aqueous phase, which deformed the lipid structure. The fusion of the lipid head groups in the dehydrated condition creates aggregated larger particles due to the loss of lamillarity (Valkova et al., 2017; Cholakova et al., 2020). The PS increased significantly at 1:10 due to a lack of adequate aqueous phase, which triggers lipid aggregation. The PS of the thermocycling siRNA-ionizable LNPs was found to be lowest with lipid–aqueous phase ratios of 1:20 and 1:30 due to optimal vapor pressure by the internal aqueous phase and solubility of the PEG-lipid. The PEG-lipids of the ionizable LNPs also played a key role in the optimization of the PS during aqueous phase change (Westesen & Siekmann, 1997; Alzorqi et al., 2016; Kumar et al., 2018). Increased aqueous phase ratio improved PEG-lipid solubility, which may also increase droplet size. With increasing aqueous phase, hydration of the head group of ionizable lipids and PEG-lipids results in increased PS, as evidenced in Table 2.

The impact of PEG–lipid concentration on PS was not the focus of our study since we emphasized on the lipid phase to mimic the FDA-approved ONPATTRO. Owing to the smallest size and narrow size distribution in PDI, 1:30 was established to be the optimal condition for the production of nano-sized thermocycling siRNA-ionizable LNPs.

4.5. Evaluation of size, potential and morphology of optimized thermocycling siRNA-ionizable LNPs

The optimized thermocycling siRNA-ionizable LNPs had a PS of 104.2 ± 34.7 nm with a PDI of 0.111 ± 0.109. The zeta potential of the siRNA-loaded thermocycle siRNA-ionizable LNPs was +21.23 ± 19.87 mV. The cryo-TEM image of the primary emulsion (Figure 7A) showed aggregated lipid droplets and a distinct electrically dense siRNA-ionizable lipid complex with insufficient encapsulation. After the 20th cycle, the aggregated lipid droplet disintegrated and the electrically dense siRNA-ionizable lipid complex was enclosed inside the spherical lipid structure (Figure 7B). The thermocycling siRNA-ionizable LNPs had an exterior layer of helper lipid and cholesterol and an electron-dense internal amorphous structure of siRNA-ionizable lipids.

Table 2. Optimization of the lipid:aqueous phase ratio for thermocycling technology.

Lipid:aqueous phase ratio	1:10	1:20	1:30	1:40	1:50
PS (nm)	147.7 ± 104.6	109.5 ± 84.9	104.2 ± 34.7	114.7 ± 14.2	134.9 ± 100.6
PDI	0.492 ± 0.216	0.215 ± 0.358	0.111 ± 0.109	0.181 ± 0.104	0.178 ± 0.283

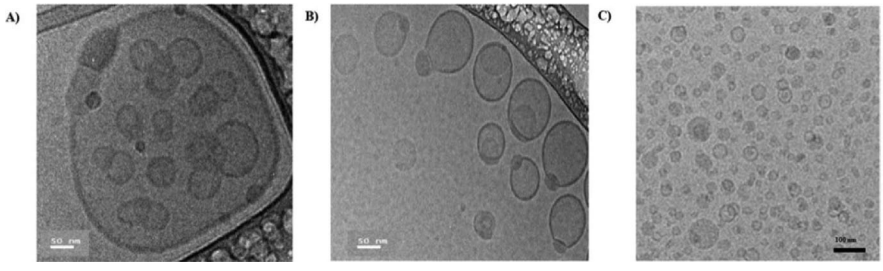

Figure 7. Cryo-TEM images of siRNA loaded thermocycle ionizable LNPs. (A) Primary emulsion of the ionizable lipids showed aggregated particles without encapsulation of the electro dens siRNA–lipid complex. (B) Optimized thermocycle technology ionizable LNPs had a spherical appearance with an evident of an amorphous electron dense core and occasional electron-lucent cavities encapsulated siRNA–ionizable lipid complex (scale bar 50 nm with magnification 25 K). (C) Cryo-TEM image of lipid nanoparticle containing siRNA and ionizable lipids similar formulated with microfluidics technology (scale bar 100 nm). Adopted from: Pieter R. Cullis et al., 2018, *On the Formation and Morphology of Lipid Nanoparticles Containing Ionizable Cationic Lipids and siRNA,* Copyright 2018 American Chemical Society.

Figure 7(C) illustrates a cryo-TEM image formulated with microfluidics technology and ionizable lipids with an N/P ratio of 6. The morphology of the 20th cycle LNPs and the microfluidics LNPs is remarkably similar (Kulkarni et al., 2018; Akinc et al., 2019), with a DSPC peripheral shell, PEG-Lipids, an internal core of electro dense ionizable lipid-siRNA complex, and cholesterol dispersed throughout (Alnylam Pharmaceuticals I, 2018; Titze-de-Almeida et al., 2020).

4.6. Evaluation of siRNA encapsulation in thermocycling ionizable LNPs

Gel electrophoresis was used to demonstrate the encapsulation ability and stability of siRNA inside thermocycle siRNA-ionizable LNPs. Figure 8(A) clearly depicts the inhibition of siRNA migration entrapped inside thermocycle ionizable LNPs (Lane 5–7). To evaluate siRNA stability throughout the thermal cycle, thermocycling siRNA-ionizable LNPs (Figure 8A lanes 2–4) were lysed with 0.2%Triton X 100 and compared to naked siRNA in Figure 8(A) Lane 1. The results demonstrated that the thermal cycle did not cause denaturation or instability of the encapsulated siRNA. These results suggest that thermocycling technology was equally as effective as microfluidics technology in the formulation of stable siRNA-ionizable LNPs without the need for organic solvents, complex multistep processes, or expensive sensitive equipment. The core-shell structure of ionizable lipids, helper lipids, cholesterol, and the PEG shell of LNPs protect anionic siRNA by forming a stable ionic combination that protects it from direct thermocycling exposure (Gujrati et al., 2014; Petrilli et al., 2016; Blakney et al., 2019; Samaridou et al., 2020).

The fluorescence intensity study (Figure 8B) was very similar to gel electrophoresis data. The maximum encapsulation rate was 83.3 ± 4.1% in the 20th cycle (Figure 8B), which was highly matched with the gel electrophoresis results. The loading of the siRNA inside the thermocycling ionizable LNPs was 3.05%. The 30th cycle showed a little drop in encapsulation, which might be related to the thermal cycle altering stability of the outer lipid membrane of thermocycle siRNA-ionizable LNPs, but the stability of the siRNA was preserved owing to the electro-dense combination of the siRNA and ionizable lipids.

4.7. Evaluation of siRNA release from thermocycling ionizable LNPs

The release of siRNA from thermocycling ionizable LNPs was carried out in PBS (pH 7.4, 10 mM, and pH 5.5, 10 mM) at 37 ± 2 °C using a dialysis tube (MWCO 25 kDa). The results in Figure 9(A,B) showed that the release of siRNA from

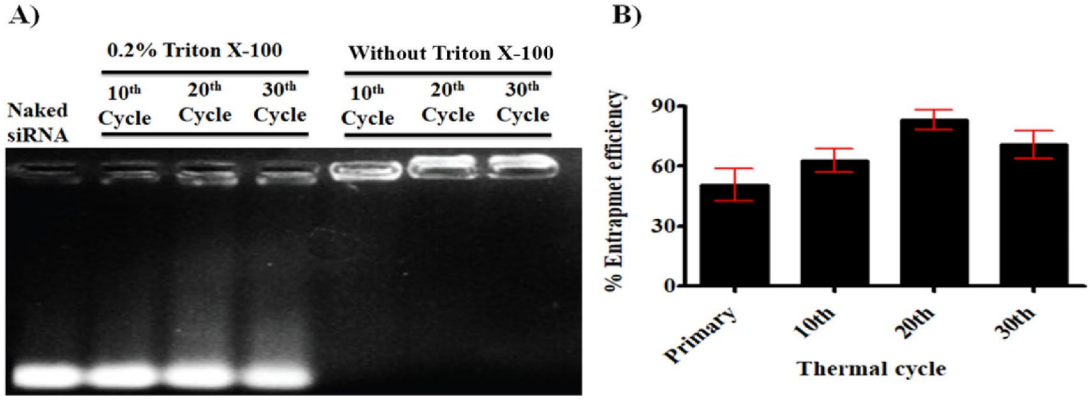

Figure 8. Encapsulation efficiency of siRNA in thermocycle ionizable LNPs. (A) Gel electrophoresis assay for analysis of siRNA encapsulation and integrity inside thermocycle technology ionizable LNPs Lane 1: naked siRNA, Lane: 2–4 0.2% Trion X 100 treated siRNA loaded ionizable LNPs lane 5–7 siRNA encapsulate ionizable LNPs. (B) % encapsulation efficiency of thermocycle technology ionizable LNPs in primary emulsion and different thermal cycle.

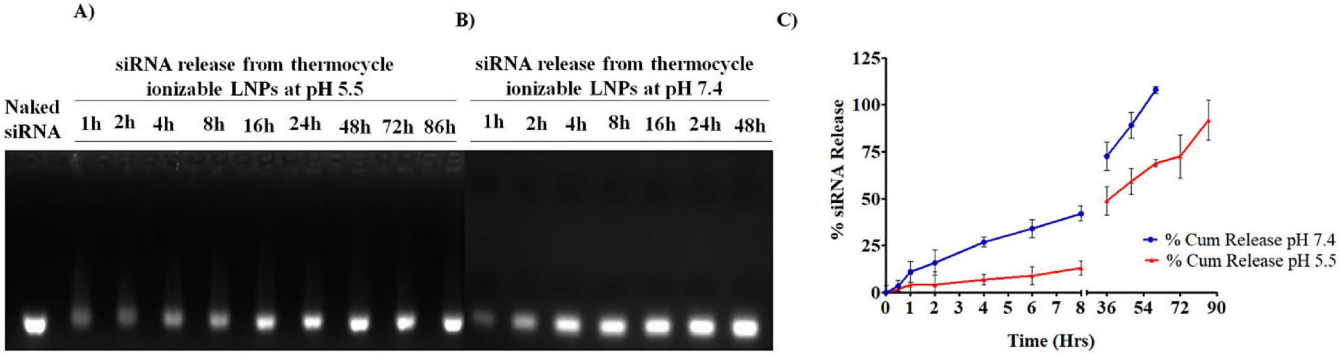

Figure 9. *In vitro* release of siRNA from thermocycling ionizable LNPs in different pH. (A) At pH 5.5, the release of siRNA is very slow. (B) pH 7.4 a fast release of siRNA occurred, indicating that the release of ionizable siRNA was pH dependent and able to endosomal escape. (C) A graphical representation of siRNA release as determined by fluoresce intensity at various pH levels.

thermocycling ionizable LNPs was pH-dependent. Figure 9(B) shows complete siRNA release at pH 7.4 for 48 hours in a control condition, but Figure 9(A) shows siRNA was not fully released and still encapsulated inside the ionizable LNPs at pH 5.5 till 86 hours. Figure 9(C) illustrates the quantification of siRNA release using the Quant-iTTM PicoGreen® reagent in correlation with gel electrophoresis data. In an acidic environment (pH 5.5), siRNA was minimally released from thermocycling ionizable LNPs indicated the escape of the endosomal pH condition. At neutral pH (≈7.4), however, the siRNA and lipids are dissociated, increasing siRNA release from thermocycling ionizable LNPs. The surface of the ionizable LNPs becomes positively charged when the endosomal pH (≈5.5) increased, interacting with the negatively charged endosomal membrane. When the pH of the solution (pH 7.4) surpasses the pKa (≈6.2) of the ionizable lipid, the ionizable lipid and siRNA become dissociated. The absence of an inner electrostatic complex between the ionizable LNPs and siRNA allowed for faster siRNA release at pH 7.4. The study by Villar-Alvarez et al. (2019) and Maugeri et al. (2019) also showed a high release of siRNA at pH 7.4 compared pH 5.0 and pH 2.0. Thermocycling LNP's ionizable lipids bind to endosomal membrane lipids, forming a water-insoluble complex salt with the siRNA encapsulated within ionizable LNPs (Wittrup et al., 2015). As a result, the lipid-siRNA complex was tightly bound together. Because such a complex salt is lipid-soluble, it might be carried along the endosomal membrane during the ionizable LNPs fusion process. When the complex reaches the cytoplasm, where the pH is neutral (≈7.4), it begins to dissociate and enhance siRNA release (Maugeri et al., 2019). Because thermocycling ionizable LNPs comprising the same ionizable lipids as ONPATTRO (Table 3), we hypothesize that a similar case of endosomal escapes of thermocycling ionizable LNPs also occurred.

4.8. Evaluation of serum stability of thermocycling siRNA-ionizable LNPs

This study focused mostly on PS, morphology, and siRNA encapsulation optimization aspects as an alternative to microfluidics technology. The study's findings on PS and siRNA loading were promising. It is crucial to investigate the stability of thermocycling siRNA-ionizable LNPs in serum and storage environments for potential *in vivo* applications. The plasma half-life of siRNA is diminished by circulating nucleases. Thermocycling siRNA-ionizable LNPs must be capable of preserving siRNA from nuclease degradation while also increasing stability and circulation half-life (Hannon & Rossi, 2004; Kim et al., 2019). The stability of loaded siRNA within thermocycling ionizable LNPs in the presence of 10% FBS at pH 7.4 at 37 ± 2 °C was investigated using gel electrophoresis, as shown in Figure 10(A–C).

Table 3. A comparable data between the thermocycling siRNA-ionizable LNPs Vs Microfluidics ONPATTRO LNPs.

Parameters	Thermocycling siRNA-ionizable LNPs	ONPATTRO Microfluidics LNPs
Composition	DLin-MC3-DMA ((6Z,9Z,28Z,31Z)-heptatriaconta-6,9, 28,31-tetraen-19-yl-4-(dimethylamino) butanoate) DMG-PEG 2000 (1,2-dimyristoyl-rac-glycero-3-m ethoxypolyethylene glycol-2000) DSPC (1,2-distearoyl-sn-glycero-3-phosphocholine) Cholesterol	DLin-MC3-DMA ((6Z,9Z,28Z,31Z)-heptatriaconta-6,9,28,31-tetraen-19-yl-4-(dimethylamino) butanoate) PEG2000-C-DMG Methoxy-Polyethylene glycol -carbamoyl-di-O-myristyl-snglyceride DSPC (1,2-distearoyl-sn-glycero-3-phosphocholine) Cholesterol (FDA, 2017; Agency EM, 2018; Alnylam Pharmaceuticals I, 2018)
Molar Ratio	50:10:38.5:1.5	50:10:38.5:1.5 (FDA, 2017; Schoenmaker et al., 2021)
N/P ratio	6	3
Morphology	Monolayers electro-dense and electro lucent spherical nanoparticles observed in cryo-TEM image	Spherical monolayered nanoparticles with a high electron density core (FDA, 2017; Kulkarni et al., 2018)
Particle size	70–130 nm	80–100 nm (FDA, 2017)
siRNA encapsulation	83%	90% (FDA, 2017; Alnylam Pharmaceuticals I, 2018)
Stability	3 months stored at 4 °C	36 months stored at −20°C (FDA, 2017)

NDA 210922 ONPATTRO (patisiran) Lipid Complex Injection; Addendum to Drug Product Quality Review (FDA, 2017; Alnylam Pharmaceuticals I, 2018).

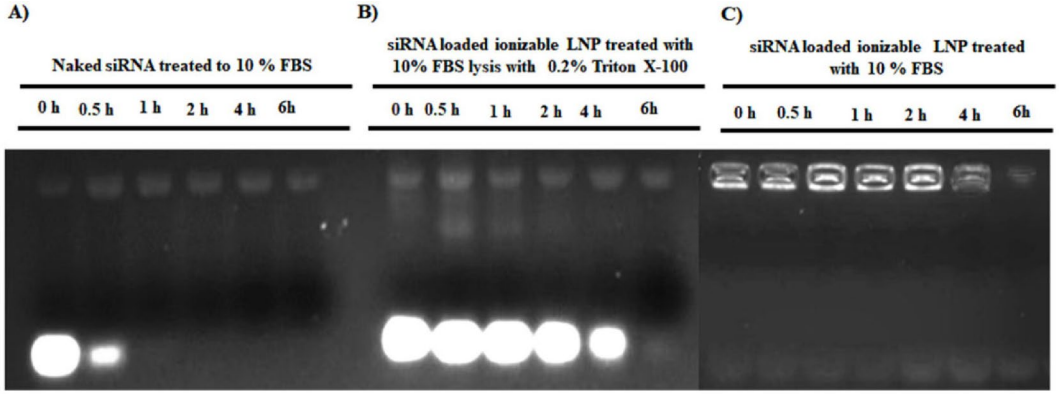

Figure 10. Serum stability of thermocycling siRNA-ionizable LNPs: Thermocycling siRNA-ionizable LNPs were incubated in 10% FBS serum at 37 °C for different time points (0, 0.5, 1, 2, 3, 4, 6 h). (A) Naked siRNA destroy within 0.5 hrs at exposure serum. (B) Released siRNA from thermocycling ionizable LNPs till 6 hrs lysis after 0.2% triton X-100 indicating the stability of siRNA in each thermal cycle. (C) Thermocycling siRNA-ionizable LNPs maintain stability of siRNA till 6 hrs at 10% FBS.

Free siRNA was destroyed by 10% FBS, but thermocycling siRNA encased inside thermocycling ionizable LNPs was completely preserved (Figure 10A,C). Figure 10B shows the integrity of the siRNA after lysis with 0.2%Triton X100. This serum stability indicated that thermocycling siRNA-ionizable LNPs were capable of sustaining the stability of the encapsulated siRNA inside the thermocycling ionizable LNPs similar to the marketed ONPATTRO LNPs.

4.9. Evaluation of storage stability of thermocycling siRNA-ionizable LNPs

The long-term stability of ionizable LNPs is the most difficult challenge in the pharmaceutical industry. To date, ultra-cold lyophilization is the only option for preserving siRNA-ionizable LNPs, but the half-life is too short (Suzuki et al., 2015; Ball et al., 2017; Evans et al., 2000; Crommelin et al., 2021; Schoenmaker et al., 2021). The FDA has authorized the storage of the COVID-19 vaccine and ONPATTRO LNPs at −80 °C and −20 °C for up to 90 days following lyophilization. For the long-term stability research, thermocycling siRNA-ionizable LNPs were kept at −21 °C (freezer), 4 °C (refrigerator), or 25 °C (room temperature). Thermocycling siRNA-ionizable LNPs were brought to room temperature for measurements and then stored at the appropriate temperature for specific time periods. The PS and PDI of thermocycling siRNA-ionizable LNPs were evaluated during a 90-day period.

Despite a little increase in z-average diameter and PDI with time, thermocycling siRNA-ionizable LNPs sustained the majority of their size and morphology after 90 days in the freezer and refrigerator, as shown in Figure 11(A,B). The thermocycling siRNA-ionizable LNPs were stable for at least 90 days after being stored at 4 °C. The lack of any organic solvent may be one of the reasons for the longer stability of the siRNA-loaded thermocycling siRNA-ionizable LNPs, which avoids physical and chemical damage to the lipids as well as the encapsulate siRNA (Gumireddy et al., 2019). Another explanation for the extended stability of thermocycling siRNA-ionizable LNPs might be the optimized thermal cycle, which retains the lipids in a stable crystalline state (Suzuki et al., 2015; Moderna, 2020). Thermal cycle stable lipid domains that preserve stability during hydrolysis and acidic environments might be another cause for thermocycling siRNA-ionizable LNPs' extended stability (Lu et al., 2019; Salminen et al., 2019). The data were correlated with the DLS using a TEM image to confirm the morphological structure of thermocycling ionizable LNPs (Figure 11C). siRNA was not stable at 25 °C (room temperature) after 4 days, as predicted. While stored at −21 °C (freezer), the siRNA-ionizable LNPs were degraded by the freezing and rehydration activities (Tang et al., 2020). ONPATTRO LNPs also advise avoiding freezing (Table 3).

5. Conclusions and future direction

The current study successfully demonstrated that a simple thermocycling technology may produce siRNA-ionizable LNPs that are as similar to microfluidics technology LNPs. The optimized settings are simple and cost-effective for producing nano-sized, highly encapsulated, and stable thermocycling siRNA-ionizable LNPs. The procedure is straightforward and well-suited to large-scale production in order to fulfill worldwide demand. With the current results and their mechanistic explanation, we attempted to open the door for the application of thermocycling technology in the formulation of nucleic acid-ionizable LNPs. Another advantageous success of thermocycling technology is the absence of any organic solvent, which boosted the stability of the siRNA within the ionizable LNPs as well as the ionizable LNPs' shelf life under refrigerated settings. Thermocycling technology was used to produce siRNA-ionizable LNPs with precise PS, shape, and encapsulation that were extremely close to commercially available microfluidic LNPs. According to our knowledge, this innovative thermocycling technology is one of the first-time approaches for the formation of siRNA-ionizable LNPs without the need for expensive equipment or organic solvents, and it is one of the most cost-effective methods for industrial scale-up. Because this is basically a proof-of-concept tool for developing a replacement for microfluidics technology, we focused our research on process optimization to achieve similar size, entrapment, and stability as microfluidics LNPs. The lipids in the thermocycling siRNA-ionizable LNPs are comparable to those in the FDA-approved ONPATTRO. We

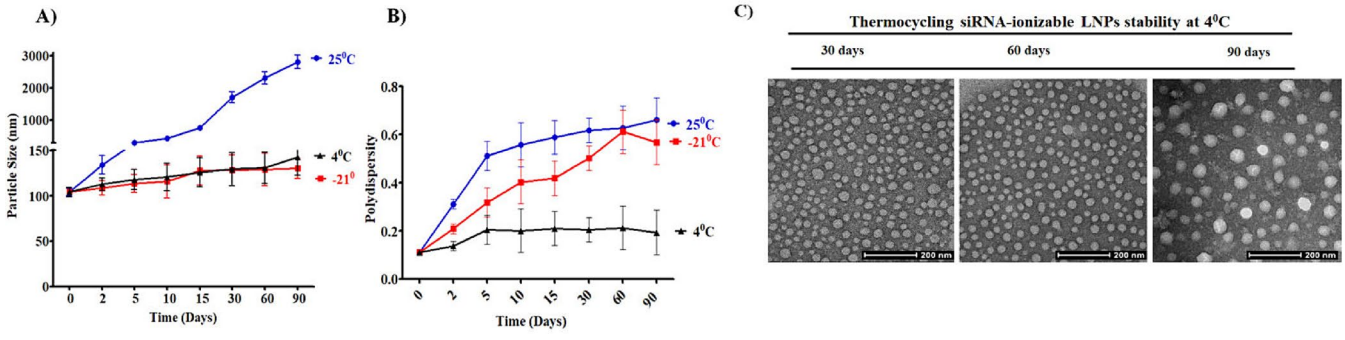

Figure 11. Stability of thermocycling siRNA–ionizable LNPs. (A) Stability of the thermocycling siRNA–ionizable LNPs PS in different storage condition for 90 days. (B) Stability of the thermocycling siRNA–ionizable LNPs PDI in different storage condition for 90 days. Thermocycling siRNA-ionizable LNPs able to retained PS and PDI in refrigerator and freezing condition. A simple refrigerator (4 °C) was capable to store thermocycling siRNA-ionizable LNPs without lyophilization for 90 days. (C) The Morphology of the thermocycling siRNA-ionizable LNPs were found unchanged till 90 days at 4 °C (scale bar = 200 nm).

expect the *in vivo* results to be similar since the thermocycling ionizable LNPs demonstrated similar *in vitro* characteristics to FDA-approved ionizable LNPs. More *in vitro* and *in vivo* research is required to assess the therapeutic effectiveness of thermocycling technology in the delivery of nucleic acid-LNPs for the management of the chronic diseases.

Disclosure statement

No potential conflict of interest was reported by the authors.

Funding

This research was supported by Basic Science Research Program through the National Research Foundation of Korea (NRF) funded by the Ministry of Science and ICT (NRF-2020R1A2B5B01001719), Korea; supported by the National Research Foundation of Korea (NRF) grant funded by the Korea government (BK 21four).

References

Abdelwahed W, Degobert G, Stainmesse S, Fessi H. (2006). Freeze-drying of nanoparticles: formulation, process and storage considerations. Adv Drug Deliv Rev 58:1688–713.

Agency EM. Summary of product characteristics: Onpattro 2 mg/mL concentrate for solution for infusion. 2018.

Akinc A, Maier MA, Manoharan M, et al. (2019). The Onpattro story and the clinical translation of nanomedicines containing nucleic acid-based drugs. Nat Nanotechnol 14:1084–7.

Alnylam Pharmaceuticals I. (2018). Alnylam Announces First-Ever FDA Approval of an RNAi Therapeutic, ONPATTRO™(patisiran) for the Treatment of the Polyneuropathy of Hereditary Transthyretin-Mediated Amyloidosis in Adults. Cambridge (MA): Alnylam Pharmaceuticals Press.

Alzorqi I, Ketabchi MR, Sudheer S, Manickam S. (2016). Optimization of ultrasound induced emulsification on the formulation of palm-olein based nanoemulsions for the incorporation of antioxidant β-d-glucan polysaccharides. Ultrason Sonochem 31:71–84.

Bakhtiar A, Neah AS, Ng KY, Chowdhury EH. (2022). In vivo evaluation of biodistribution and toxicity of pH-responsive strontium nanoparticles for gene delivery. J Pharm Investig 52:95–107.

Ball RL, Bajaj P, Whitehead KA. (2017). Achieving long-term stability of lipid nanoparticles: examining the effect of pH, temperature, and lyophilization. Int J Nanomedicine 12:305–15.

Blakney AK, McKay PF, Yus BI, et al. (2019). Inside out: optimization of lipid nanoparticle formulations for exterior complexation and in vivo delivery of saRNA. Gene Ther 26:363–72.

Buyens K, Demeester J, De Smedt SS, Sanders NN. (2009). Elucidating the encapsulation of short interfering RNA in PEGylated cationic liposomes. Langmuir 25:4886–91.

Chae Y-J, Chang J-E, Lee M-K, et al. (2022). Regulation of drug transporters by microRNA and implications in disease treatment. J Pharm Investig 52:23–5.

Cholakova D, Glushkova D, Tcholakova S, Denkov N. (2020). Nanopore and nanoparticle formation with lipids undergoing polymorphic phase transitions. ACS Nano 14:8594–604.

Chuesiang P, Siripatrawan U, Sanguandeekul R, et al. (2018). Optimization of cinnamon oil nanoemulsions using phase inversion temperature method: impact of oil phase composition and surfactant concentration. J Colloid Interface Sci 514:208–16.

Crommelin DJ, Anchordoquy TJ, Volkin DB, et al. (2021). Addressing the cold reality of mRNA vaccine stability. J Pharm Sci 110:997–1001.

Cui L, Pereira S, Sonzini S, et al. (2022). Development of a high-throughput platform for screening lipid nanoparticles for mRNA delivery. Nanoscale 14:1480–91.

Cui L. (2015). Lipopolyplexes containing bifunctional peptides for DNA and siRNA delivery: Doctoral dissertation. England, UK: King's College London.

Cun D, Foged C, Yang M, et al. (2010). Preparation and characterization of poly (DL-lactide-co-glycolide) nanoparticles for siRNA delivery. Int J Pharm 390:70–5.

Denkov N, Tcholakova S, Lesov I, et al. (2015). Self-shaping of oil droplets via the formation of intermediate rotator phases upon cooling. Nature 528:392–5.

Evans RK, Xu Z, Bohannon KE, et al. (2000). Evaluation of degradation pathways for plasmid DNA in pharmaceutical formulations via accelerated stability studies. J Pharm Sci 89:76–87.

Evers MJ, Kulkarni JA, van der Meel R, et al. (2018). State-of-the-art design and rapid-mixing production techniques of lipid nanoparticles for nucleic acid delivery. Small Methods 2:1700375.

FDA. (2017). FDA ONPATTRO (patisiran) Lipid Complex Injection Addendum to Drug Product Quality Review [WWW Document]. Available at: https://www.accessdata.fda.gov/drugsatfda_docs/nda/2018/210922Orig1s000ChemR.pdf.

Forigua A, Kirsch RL, Willerth SM, Elvira KS. (2021). Recent advances in the design of microfluidic technologies for the manufacture of drug releasing particles. J Control Release 333:258–68.

Golmohammadzadeh S, Mokhtari M, Jaafari MR. (2012). Preparation, characterization and evaluation of moisturizing and UV protecting effects of topical solid lipid nanoparticles. Braz J Pharm Sci 48:683–90.

Gujrati M, Malamas A, Shin T, et al. (2014). Multifunctional cationic lipid-based nanoparticles facilitate endosomal escape and reduction-triggered cytosolic siRNA release. Mol Pharm 11:2734–44.

Gumireddy A, Christman R, Kumari D, et al. (2019). Preparation, characterization, and in vitro evaluation of curcumin-and resveratrol-loaded solid lipid nanoparticles. AAPS PharmSciTech 20:1–14.

Hannon GJ, Rossi JJ. (2004). Unlocking the potential of the human genome with RNA interference. Nature 431:371–8.

Jones KL, Drane D, Gowans EJ. (2007). Long-term storage of DNA-free RNA for use in vaccine studies. Biotechniques 43:675–81.

Karnik R, Gu F, Basto P, et al. (2008). Microfluidic platform for controlled synthesis of polymeric nanoparticles. Nano Lett 8:2906–12.

Kim B, Park JH, Sailor MJ. (2019). Rekindling RNAi therapy: materials design requirements for in vivo siRNA delivery. Adv Mater 31:1903637.

Kulkarni JA, Darjuan MM, Mercer JE, Chen S, et al. (2018). On the formation and morphology of lipid nanoparticles containing ionizable cationic lipids and siRNA. ACS Nano 12:4787–95.

Kumar R, Singh A, Garg N, Siril PF. (2018). Solid lipid nanoparticles for the controlled delivery of poorly water soluble non-steroidal anti-inflammatory drugs. Ultrason Sonochem 40:686–96.

Kundu AK, Chandra PK, Hazari S, et al. (2012). Development and optimization of nanosomal formulations for siRNA delivery to the liver. Eur J Pharm Biopharm 80:257–67.

Kwon HJ, Kim S, Kim S, et al. (2017). Controlled production of monodisperse polycaprolactone microspheres using flow-focusing microfluidic device. BioChip J 11:214–8.

Lu X, Fang C, Sheng X, et al. (2019). One-step and solvent-free synthesis of polyethylene glycol-based polyurethane as solid–solid phase change materials for solar thermal energy storage. Ind Eng Chem Res 58:3024–32.

Maugeri M, Nawaz M, Papadimitriou A, et al. (2019). Linkage between endosomal escape of LNP-mRNA and loading into EVs for transport to other cells. Nat Commun 10:1–15.

Moderna. (2020). Moderna announces longer shelf life for its COVID-19 vaccine candidate at refrigerated temperatures. Cambridge, MA: Moderna. Inc.

Pardi N, Hogan MJ, Porter FW, Weissman D. (2018). mRNA vaccines—a new era in vaccinology. Nat Rev Drug Discov 17:261–79.

Petrilli R, Eloy JO, de Souza MC, et al. (2016). Lipid nanoparticles as non-viral vectors for siRNA delivery: concepts and applications. In: Nanobiomaterials in drug delivery. Norwich New York, USA: Elsevier, 75–109.

Roces CB, Lou G, Jain N, et al. (2020). Manufacturing considerations for the development of lipid nanoparticles using microfluidics. Pharmaceutics 12:1095.

Ryu S, Jin M, Lee H-K, et al. (2022). Effects of lipid nanoparticles on physicochemical properties, cellular uptake, and lymphatic uptake of 6-methoxflavone. J Pharm Investig 52:233–41.

Salminen H, Ankenbrand J, Zeeb B, et al. (2019). Influence of spray drying on the stability of food-grade solid lipid nanoparticles. Food Res Int 119:741–50.

Samaridou E, Heyes J, Lutwyche P. (2020). Lipid nanoparticles for nucleic acid delivery: Current perspectives. Adv Drug Deliv Rev 154-155:37–63.

Sato K. (2018). Crystallization of lipids: fundamentals and applications in food, cosmetics, and pharmaceuticals. Hoboken, NJ: John Wiley & Sons.

Schoenmaker L, Witzigmann D, Kulkarni JA, et al. (2021). mRNA-lipid nanoparticle COVID-19 vaccines: structure and stability. Int J Pharm 601:120586.

Shepherd SJ, Issadore D, Mitchell MJ. (2021). Microfluidic formulation of nanoparticles for biomedical applications. Biomaterials 274:120826.

Sriwongsitanont S, Ueno M. (2010). Effect of freeze-thawing process on the size and lamellarity of peg-lipid liposomes. Open Colloid Sci J 4(1):1–6.

Suzuki Y, Hyodo K, Tanaka Y, Ishihara H. (2015). siRNA-lipid nanoparticles with long-term storage stability facilitate potent gene-silencing in vivo. J Control Release 220:44–50.

Tang M, Hu S, Hattori Y. (2020). Effect of pre-freezing and saccharide types in freeze-drying of siRNA lipoplexes on gene-silencing effects in the cells by reverse transfection. Mol Med Rep 22:3233–44.

Tcholakova S, Valkova Z, Cholakova D, et al. (2017). Efficient self-emulsification via cooling-heating cycles. Nat Commun 8:15012.

Titze-de-Almeida SS, Brandão PRdP, Faber I, Titze-de-Almeida R. (2020). Leading RNA interference therapeutics part 1: silencing hereditary transthyretin amyloidosis, with a focus on patisiran. Mol Diagn Ther 24:49–59.

Trenkenschuh E, Friess W. (2021). Freeze-drying of nanoparticles: how to overcome colloidal instability by formulation and process optimization. Eur J Pharm Biopharm 165:345–60.

Tsao C-W. (2016). Polymer microfluidics: Simple, low-cost fabrication process bridging academic lab research to commercialized production. Micromachines 7:225.

Valkova Z, Cholakova D, Tcholakova S, et al. (2017). Mechanisms and control of self-emulsification upon freezing and melting of dispersed alkane drops. Langmuir 33:12155–70.

Vandamme TF, Anton N. (2010). Low-energy nanoemulsification to design veterinary controlled drug delivery devices. Int J Nanomedicine 5:867–73.

Villar-Alvarez E, Leal BH, Martinez-Gonzalez R, et al. (2019). SiRNA silencing by chemically modified biopolymeric nanovectors. ACS Omega 4:3904–21.

Westesen K, Siekmann B. (1997). Investigation of the gel formation of phospholipid-stabilized solid lipid nanoparticles. Int J Pharm 151:35–45.

Wittrup A, Ai A, Liu X, et al. (2015). Visualizing lipid-formulated siRNA release from endosomes and target gene knockdown. Nat Biotechnol 33:870–6.

Zhang N-N, Li X-F, Deng Y-Q, et al. (2020). A thermostable mRNA vaccine against COVID-19. Cell 182:1271–83. e16.

Zhao P, Hou X, Yan J, et al. (2020). Long-term storage of lipid-like nanoparticles for mRNA delivery. Bioact Mater 5:358–63.